Expert Systems with Applications 39 (2012) 11183–11193

Contents lists available at SciVerse ScienceDirect

Expert Systems with Applications

journal homepage: www.elsevier.com/locate/eswa

Use of discrete gradient operators for the automatic determination of vanishing points: Comparative analysis

José Ignacio Rojas-Sola [a,*], Antonio Romero-Manchado [b]

[a] University of Jaen, Department of Engineering Graphics, Design and Projects, Campus de las Lagunillas, Jaen 23071, Spain
[b] University of Jaen, Department of Cartographic Engineering, Geodesy and Photogrammetry, Campus de las Lagunillas, Jaen 23071, Spain

ARTICLE INFO

Keywords:
Vanishing point
Thales' second theorem
Monoscopic image
Discrete gradient operators

ABSTRACT

Thales' second theorem can be used for the automatic detection of the vanishing points of an image. This paper explores its reliability and accuracy according to the type of operator used for the detection of edges. An algorithm has been used which processes a photographic image according to the operator selected. The result is a point cloud which is then used to find the desired solution. The comparison between the four discrete gradient operators (Frei-Chen, Prewitt, Roberts and Sobel) has been made taking into account the resolution of the image and the number of vanishing points. The results obtained show that Frei-Chen's operator shows good performance in determining vanishing points with respect to the spatial *X* axis, Sobel's operator is the best for determining the vanishing point with respect to the spatial *Y* axis, Roberts' operator gives good results for calculating vanishing points in both spatial axes, and Prewitt's operator is not appropriate for processing this type of image.

1. Introduction

A monoscopic image is a projection of a three-dimensional scene on a plane, which is performed using a viewpoint and can be expressed as a perspective. However, although the third dimension is apparently lost during this projection, it can be retrieved if the stored information is treated appropriately using photogrammetric techniques or dimensional perspective analysis.

Historically, perspective has been studied by artists seeking to represent more faithfully three-dimensional scenes on flat materials (paintings or prints, among others), but nowadays studies are focused on the three-dimensional representation of objects from a bi-dimensional image.

The most well-known perspective effect is that in space parallel lines converge at a common point known as a vanishing point, and if the set of lines is parallel to one of the three main axes (*X*, *Y*, *Z*), this point is known as a main vanishing point. Knowledge of these points gives information about elements of an image, which means that a qualitative and/or quantitative analysis of the image can be carried out. Qualitatively, vanishing points can be used to group common lines in adjacent images which need to be merged, and quantitatively, vanishing points are used for automatic calibration of a camera, dimensional analysis of an object or three-dimensional reconstruction.

Therefore, it is very important to define the reliability of the methods and operators used in the detection of vanishing points, and this is one of the main objectives of this research.

1.1. Background

Calculating vanishing points is the nucleus of the majority of modeling work based on a single image. However, the difficulty in determining the position of these points lies in the search for a computational technique which is accurate, reliable, quick and simple. Despite the research carried out until now, the methods which have been developed to detect vanishing points fulfill only some of these characteristics.

Barnard (1983) used the Gaussian sphere instead of gradient space as domain for representing geometric constraints. The Gaussian sphere is symmetric with respect to the view point (in the same way as central or perspective projection) whereas the symmetry of gradient space is the same as orthographic projection. In addition, the use of a closed or finite space such as a sphere as opposed to an open or infinite space such as that of the gradient has advantages from a computational point of view.

Magee and Aggarwal (1984) developed a computationally inexpensive algorithm for the determination of vanishing points, both on an image plane or in the infinite. For this, the algorithm uses a series of cross-product operations in order to determine that point toward the intersection of line segments in the image plane. These vectors are represented and parameterized on the Gaussian

* Corresponding author. Tel.: +34 953 212452; fax: +34 953 212334.
E-mail address: jirojas@ujaen.es (J.I. Rojas-Sola).

0957-4174/$ - see front matter © 2012 Elsevier Ltd. All rights reserved.
http://dx.doi.org/10.1016/j.eswa.2012.03.059

sphere. Finally, the number of entries for a given pair of parameters (α, β) is counted, and if the number is large enough, the lines that contributed to the pair are shown.

For Collins and Weiss (1990), the vanishing point computation is characterized as a statistical estimation problem on the unit sphere; in particular as the estimation of the polar axis of an equatorial distribution. For this, the image line segments are previously clustered into groups of convergent lines.

Palmer and Tai (1993) use the Hough transform algorithm to determine the parameters of the lines which intersect to form the vanishing points. In order to measure the accuracy a post-processing of the segments of the straight lines is carried out in order to reject those with greater uncertainty in their parameters.

Straforini, Coelho, and Campani (1993) propose a previous selection of points which converge at a given vanishing point in order to reduce the computational cost associated with the detection of the vanishing point. The solution is to use a polar space in which each line is represented by a point, which allows them to be grouped with a minimal computational cost.

Tai, Kittler, Petrou, and Windeatt (1993) use combinations of three lines whose intersections provide points which may be vanishing points. This method provides probability measures which reflect the likelihood of those points being the vanishing points, and the advantage of this method is that it allows the identification of vanishing points in less structured environments.

McLean and Kotturi (1995) present a method for the detection of vanishing points based on sub-pixel line descriptions which recognizes the existence of errors in feature detection and which does not rely on supervision or the arbitrary specification of thresholds.

Gamba, Mecocci, and Salvatore (1996) designed a vanishing point detection algorithm for non-structured scenes. In the first step, infinite distance vanishing points are detected by simplifying the successive search, that is, all the segments parallel to the plane of the photograph are detected (vertical and horizontal directions). In the following step the rest of the segments are classified according to the vanishing point they belong to, and the cloud obtained is represented using their intersections. A voting scheme is applied to this cloud to rule out incorrect points or those which cannot be the vanishing point.

Schaffalitzky and Zisserman (2000) showed that by grouping the characteristics of an object which provide a geometric relationship it is possible to automate the determination of the vanishing points of the image. For this, they use geometric grouping algorithms which allow the unsupervised detection of the vanishing point.

Almansa, Desolneux, and Vamech (2003) developed a detection algorithm that relies on the Helmotlz principle. This vanishing points detector has a high degree of accuracy, and does not need information about the image of the parameters of the camera.

Kalantari, Jung, Paparoditis, and Guedon (2008) proposed an extraction method for vanishing points of an image obtained with a camera with unknown internal orientation parameters. In order to find the vanishing points the perspective of the camera is located, where the Gaussian sphere is situated, at a standard orthogonal distance from the image plane. This algorithm works in a similar way to monocular human vision, which allows the mental reconstruction of the vanishing points with no prior optical information.

Kalantari, Jung, and Guedon (2009) presented a method based on Thales' second theorem for the automatic and simultaneous detection of an image's vanishing points. Each vanishing point is associated with a circle which relates to a point cloud, which allows the automation of the process. However, this method is only applicable in urban environments.

1.2. Objectives

The objectives of this research are:

1. To show the different methods of detection of vanishing points in scientific literature.
2. To select a detection method for vanishing points in order to assess is effectiveness in photographic images with one and two vanishing points.
3. To develop an algorithm based on the selected method: Thales' second theorem (Kalantari et al., 2009).
4. To analyze the influence of the type of operator selected for edge detection in the results obtained, specifically the discrete gradient operators of Frei-Chen, Prewitt, Roberts and Sobel.

In order to fulfill these objectives this paper is organized as follows. In Section 2, the materials used are presented along with the methodology followed. The stages of work are established, with a flow diagram of the algorithm developed for the detection of vanishing points, and each stage is explained. Then, in Section 3, the results are presented after the algorithm if applied to photographs with one and two vanishing points. Some discussions relating to the type of operator used are given in Section 4 using box plot graphics. Section 5 concludes the paper.

2. Material and methods

2.1. Object selection and material used

In order to carry out this research it has been necessary to take a series of representative photographs in which the algorithm will be applied. These photographs are perspectives with one and two vanishing points. In order for their detection to be possible, the photographs have to contain simple geometric forms such as straight lines. From the geometric characteristics of straight lines in perspective, it is possible to define the position of the vanishing points of the photographic perspective.

Building C5 of the University of Jaen Campus has been chosen (Fig. 1), as it has a very define geometric structure. The design of the façade is composed of parallel and perpendicular lines, which can be aligned according to the three axes of spatial coordinates (X, Y, Z), allowing the photographic viewpoint to be situated in the appropriate place with respect to the object.

The photographs were taken with a Nikon reflex camera, model D200, with a maximum resolution of 3872×2592 pixels, and with an Olympus compact camera, model Olympus-μ5000, with a maximum resolution of 3968×2976 pixels.

2.2. Stages of work

The research was carried out in the following stages:

1. Data collection: In this stage the object to be studied is selected, and the location and orientation of the photographic viewpoints are determined, according to the desired vanishing points. The photographs are taken.
2. Data processing: The photographs are analyzed and processed with a vanishing point detection algorithm (VPD), implemented in Borland Delphi 7.0. The flow diagram is shown in Fig. 2.
3. Analysis of results: Knowledge of the edge operator selected in the results obtained is crucial to discriminate its use according to the characteristics of the image, and therefore, it is important to know which type of operator performs best

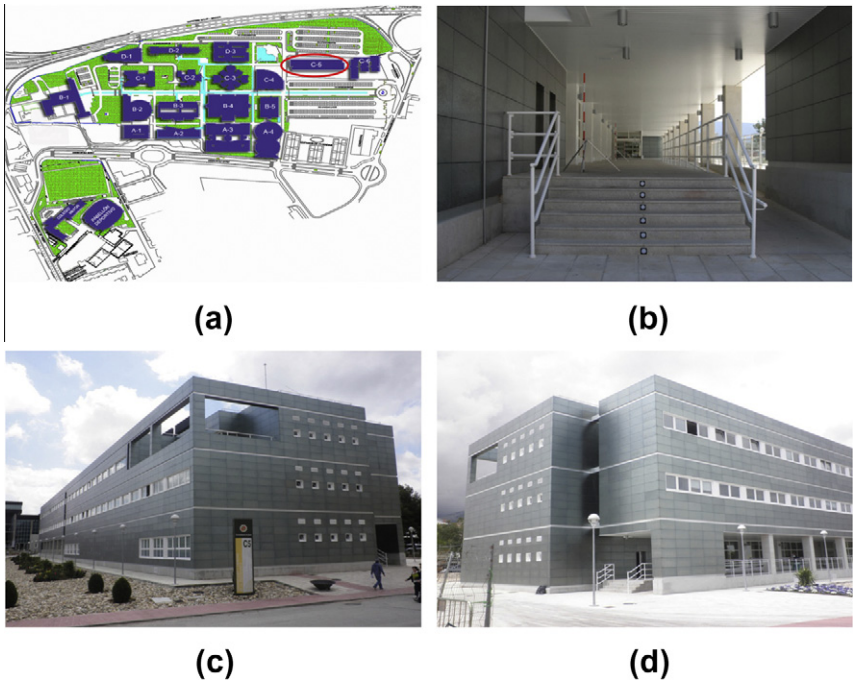

Fig. 1. (a) Map of the University of Jaen campus and location of building C5 (www.ujaen.es). (b) Photograph of the south-facing façade: perspective with one vanishing point. (c) Photograph of the north and east facades: perspective with two vanishing points. (d) Photograph of the south and east facades: perspective with two vanishing points.

according to the vanishing point to be determined. At the same time, analysis is carried out into how resolution influences the results.

2.2.1. Description of the algorithm used

The algorithm has been developed in Borland Delphi. This is a powerful tool which is easy to use to develop applications in Windows, which allows programming oriented towards objects, using a high level language such as Object Pascal. Therefore, it allows the development of complex applications without the need to know C and C++.

The computational requirements of the algorithm allow it to be used in 32 and 64-bit platforms in Windows XP, Vista or 7.

2.2.2. Edge detection

In general, edges refer to something physical, formed either by the shape of three-dimensional objects or by the properties of materials. In geometric terms, there are two types of physical edges: the set of points along which there is an abrupt change in the orientation of the physical surface, or the set of points which show the limit between two or more materially different regions of the physical surface (Bovik, 2009).

However, in a photographic image the edges may be different from physical edges, as they are in a perspective projection. Therefore, an edge can be defined as a limit which separates adjacent regions of the image which have different characteristics in the same feature of interest, either luminance (gray level), reflectance, color or texture.

For example, in the case of luminance, the pixels of the edge are those which are located in a sharp change of the gray level, giving a new image which shows the classification of the edge pixels and the attributes of the edge, that is, magnitude and orientation.

Edge-detection methods can be classified into three types: Gradient-based, Laplacian-based and Canny. However, in order to make this research briefer, the performance of only four gradient operators will be analyzed, applied to the discrete space of the image: Roberts (2×2), Prewitt (3×3), Sobel (3×3) and Frei-Chen (3×3).

2.2.3. Segmentation of the gradient orientation

Using the operators indicated in the previous section, for each pixel the magnitude and orientation of the local gradient is calculated. This allows the pixels to be grouped into regions which, although they have a local similarity, may include pixels with a very different orientation, owing to a slight discrepancy in the orientation of one pixel to another at corners or joins between straight lines.

A possible solution is to perform grouping by using fixed partitions in the space of the gradient orientation (Fig. 3), with each gradient vector labeled and assigned to a single partition. In this way, the pixels which are included in the lineal context of a straight line will be from the same partition. However, the use of a fixed partition causes problems with the location of the edges of fixed partitions and the resulting lack of sensitivity to possible distributions of the directions of the edges. For example, visually distinct straight lines which are spatially adjacent may be inappropriately combined because they have similar orientations and belong to the same grouping. In addition, if the distribution of orientations of the gradient is at the edge of a partition, a straight line may produce fragmented support regions.

Burns, Hanson, and Riseman (1986) propose the use of two sets of fixed overlapping partitions (Fig. 3), so that when a partition fragments a line because it is on the edge of a partition, the other will be located within a partition without fragmenting it (Fig. 4).

2.2.4. Line extraction

Once the extraction of the line support regions has been performed, the parameters which represent the straight line they contain are obtained, as the estimated gradient shares a common orientation.

The main axis of a support region allows us to obtain a fitted line without increasing the complexity of the algorithm. To do this, it is possible to use the method proposed by Wang, Lin, and Chen

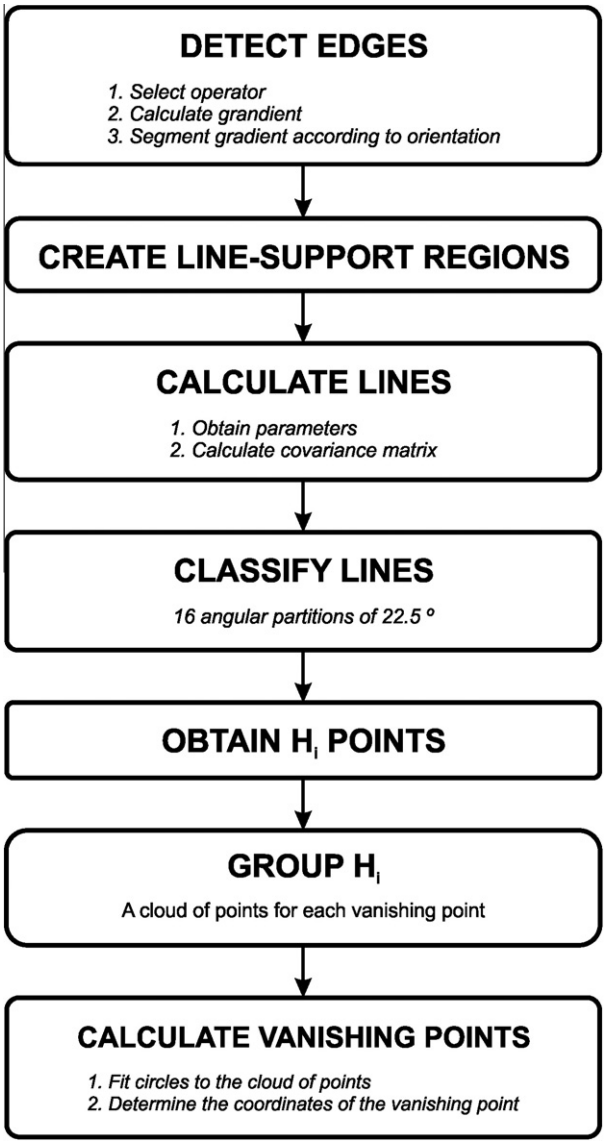

Fig. 2. Flow diagram of the VPD algorithm.

(2010) or by Kang and Jung (2003). For reasons of simplicity and speed of calculation, the straight line associated with the line support region has been defined by determining the coordinates of the center (x_c,y_c) and their orientation (θ_s) (Kang & Jung, 2003). It is also necessary to calculate the covariance matrix of each line to use it in the following stages of the algorithm.

2.2.5. Obtaining the point cloud H_i

By applying Thales' second theorem to the set of lines extracted, a point cloud H_i is obtained. Fig. 5 shows the correspondence of its spatial distribution with three circumferences which pass through the adopted origin of the coordinates (upper left corner of the image). Each of these circumferences corresponds to a vanishing point.

2.2.6. Fitting circles to the point cloud H_i

This stage is the central point of the method, as the vanishing points are located on the circles defined by the point cloud H_i. The circles are obtained following this sequence:

1. Classify the point cloud H_i obtained according to the vanishing point they belong to, using the orientation values of the straight lines and their classification according to the angular partition adopted (16 partitions of 22.5°).
2. Create a space with point accumulation, establishing a minimum cell size which is calculated according to the horizontal and vertical resolution of the image. In each cell the points are counted, which can be used to filter points.
3. For each sub-cloud of points:
   - 3.1. Calculate the average value (x_m,y_m) and their dispersion (σ_x,σ_y).
   - 3.2. Fit an initial circle using the algebraic distance minimization method (Gander, Golub, & Strebel, 1994), taking as points the origin (0,0), the average value of the point cloud (x_m,y_m) and a third point with coordinates $(x_m \pm \sigma_x, y_m \pm \sigma_y)$, according to the vanishing point.
   - 3.3. Fit circles using the algebraic distance minimization method (Gander et al., 1994), using the previous circle as an approximation. The number of iterations necessary will depend on the number of accumulation cells which contain points. The first circle is made with the cell with the highest number of points, the second with the two cells with most points, and so on. In all calculations the origin (0,0) is included.

Although this method differs from that proposed by Kalantari et al. (2009) (Fig. 6a), it improves the repetition of the results by eliminating the random selection of points to carry out the initial approximation (Fig. 6b).

2.2.7. Calculation of the vanishing point coordinates

Before calculating the vanishing point coordinates it is necessary to select the circles which fit best the point cloud H_i, and therefore which provide the best approximation to the vanishing points coordinates.

Kalantari et al. (2009) suggest that the origin of the fitted circles should be the centroid of the circles detected in the previous step.

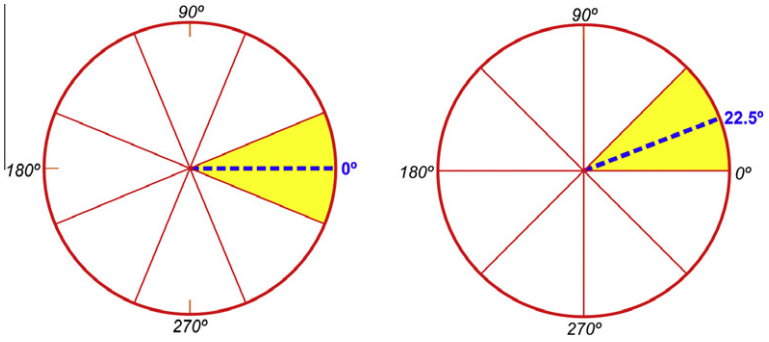

Fig. 3. Diagram showing fixed angular partitions of the orientation space of the gradient: eight partitions of 45°. (Left) Centering the first partition on 0°. (Right) Centering the first partition on 22.5°.

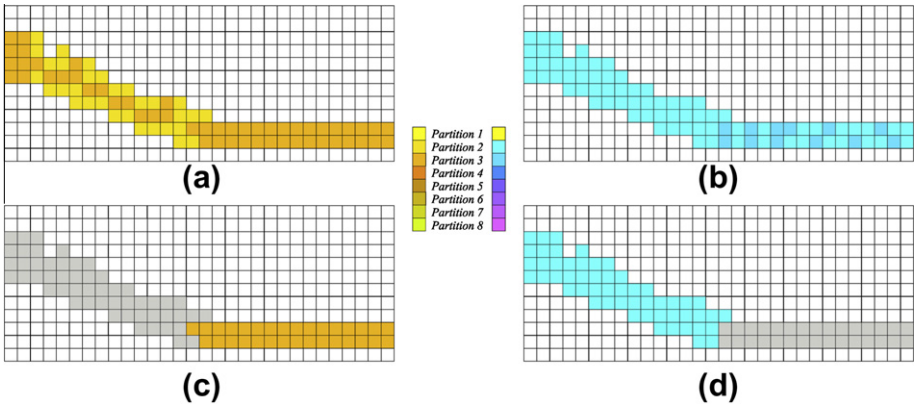

Fig. 4. Application of the double partition technique. (a) Result of eight partitions of 45° with the first sector centered on 0°. (b) Result of the same partitions but with the first sector centered on 22.5°. (c) Elimination of the support regions in (a) with a size smaller than 50%. (d) Elimination of the support regions in (b) with a size smaller than 50%.

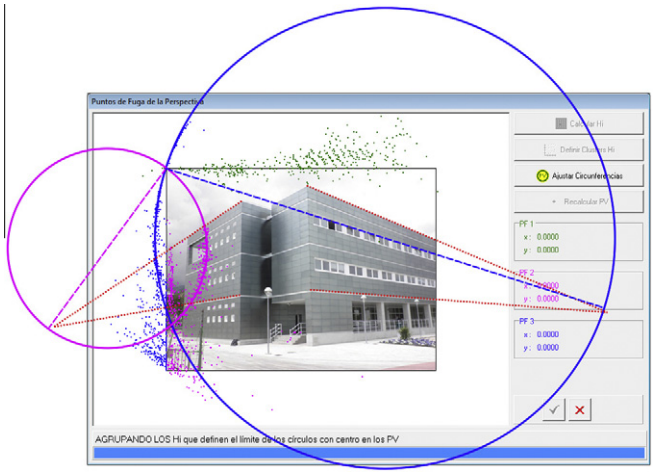

Fig. 5. Application of the method proposed by Kalantari et al. (2009) to an image with two vanishing points. The point cloud has been obtained from lines extracted by applying Prewitt's operator. The intersection of the lines of points shows the approximate location of the vanishing points. The broken line indicates the positions of the vanishing points after fitting the circles to the point cloud.

Here it is proposed to select the circle which contains the greatest number of points H_i in a band around the circle, the thickness of which is defined by expression (1):

$$\varepsilon = \operatorname{median} a_i \times \sqrt{\frac{1}{2}\left(\sigma^2_{H_{i,x}} + \sigma^2_{H_{i,y}} + \sqrt{\left(\sigma^2_{H_{i,x}} + \sigma^2_{H_{i,y}}\right)^2 - 4\left(\sigma^2_{H_{i,x}}\sigma^2_{H_{i,y}} - \sigma^2_{H_{i,x}H_{i,y}}\right)}\right)} \quad (1)$$

Fig. 7. Comparative view of the result of the algorithm for an image with one vanishing point according to the type of operator. The vanishing point is located on the spatial Y axis.

where ε is the median of the semi axes of the error ellipse of all the H_i points associated with a vanishing point. Its value, therefore, depends directly on the accuracy with which the H_i points have been determined, which allows the process to be automated.

Once the circle and the associated point cloud H_i have been determined, a new fit is carried out, applying the mathematical model of minimization of geometric distance (2):

$$F(X_c, X_{H_i}) = \left(\|\overline{X}_c - \overline{X}_{H_i}\| - \|\overline{X}_C\|\right) \quad (2)$$

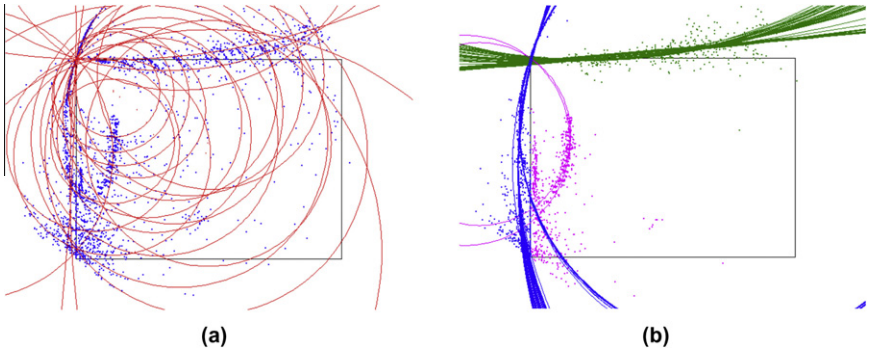

Fig. 6. (a) Fitting circles using the method proposed by Kalantari et al. (2009) to Fig. 1(d). (b) Fitting of circles using the variation of the proposed method.

Fig. 8. Comparative view of the result of the algorithm for an image with two vanishing points (case 1) according to the type of operator. The vanishing points are located on the spatial *X* axis (right) and *Y* axis (left).

Fig. 9. Comparative view of the result of the algorithm for an image with two vanishing points (case 2) according to the type of operator. The vanishing points are located on the spatial *X* axis (right) and *Y* axis (left).

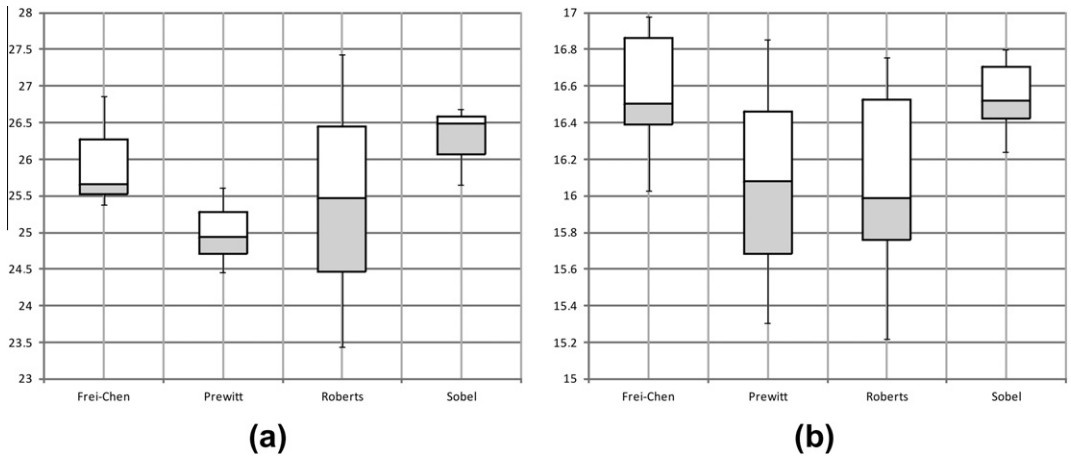

Fig. 10. Box-plot graphics of the coordinates of the vanishing point corresponding to the spatial *Y* axis. The *x* coordinate is shown in (a) and the *y* coordinate in (b). Values in millimeters.

The final coordinates of the vanishing point (VP) are easily calculated as they are located on the diameter which has one of its sides in the origin (upper left corner of the image). Therefore, the coordinates of the vanishing point are obtained by applying expressions (3) and (4):

$$X_{VP} = 2 * X_C \tag{3}$$

$$Y_{VP} = 2 * Y_C \tag{4}$$

where (X_C, Y_C) are the coordinates of the center of the circle.

3. Results

This section shows a sample of the results obtained by applying the algorithm developed on photographs with one vanishing point (spatial *Y* axis) and with two vanishing points (spatial *X* and *Y* axes). It has been considered that the vanishing point corresponding to the *Z* axis is in the infinite, and therefore the results are not taken into account in the analysis.

Figs. 7–9 show the position obtained for two vanishing points according to the operator used (Frei-Chen, Prewitt, Roberts and So-

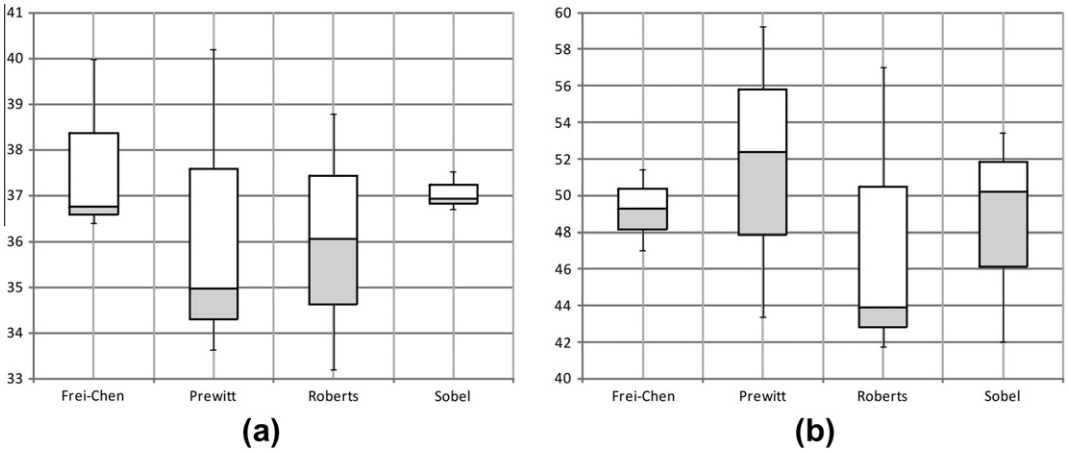

Fig. 11. Box-plot graphics of the coordinates of the vanishing point corresponding to the spatial *X* axis. The *x* coordinate is shown in (a) and the *y* coordinate in (b). Values in millimeters.

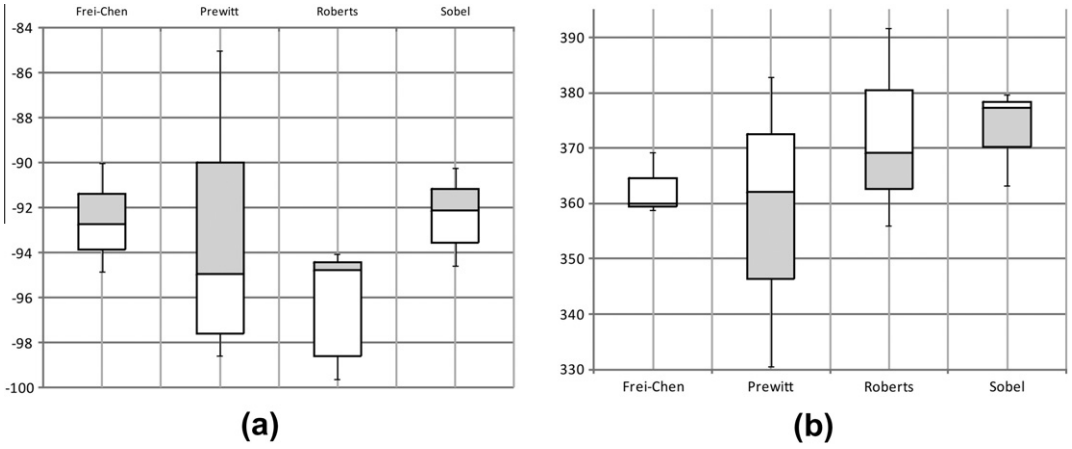

Fig. 12. Box-plot graphics of the coordinates of the vanishing point corresponding to the spatial *Y* axis. The *x* coordinate is shown in (a) and the *y* coordinate in (b). Values in millimeters.

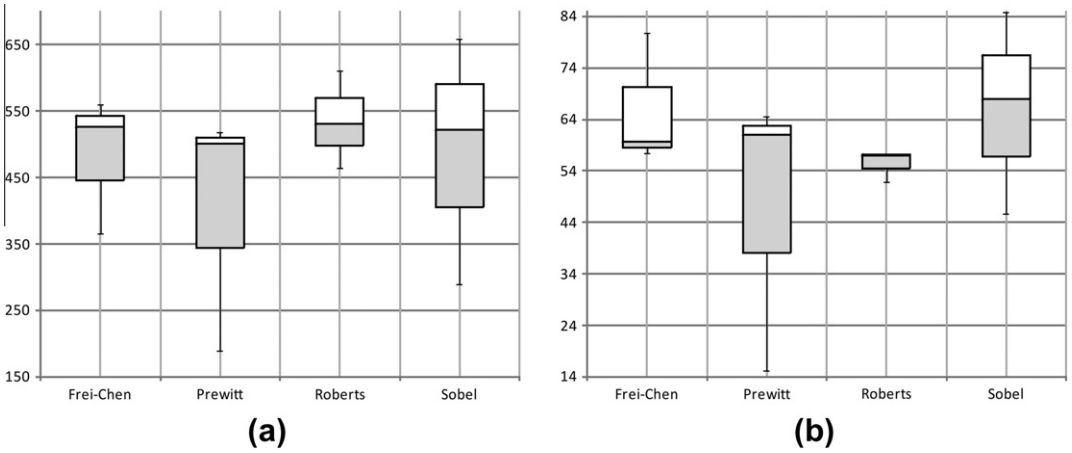

Fig. 13. Box-plot graphics of the coordinates of the vanishing point corresponding to the spatial *X* axis. The *x* coordinate is shown in (a) and the *y* coordinate in (b). Values in millimeters.

bel), as well as the approximate location found manually by the intersection of straight lines. The statistical study of these results and of those obtained when the image resolution is varied is shown in Section 4.

4. Discussion

This section analyses the results obtained after applying the four edge operators to the three photographs above. The discussion

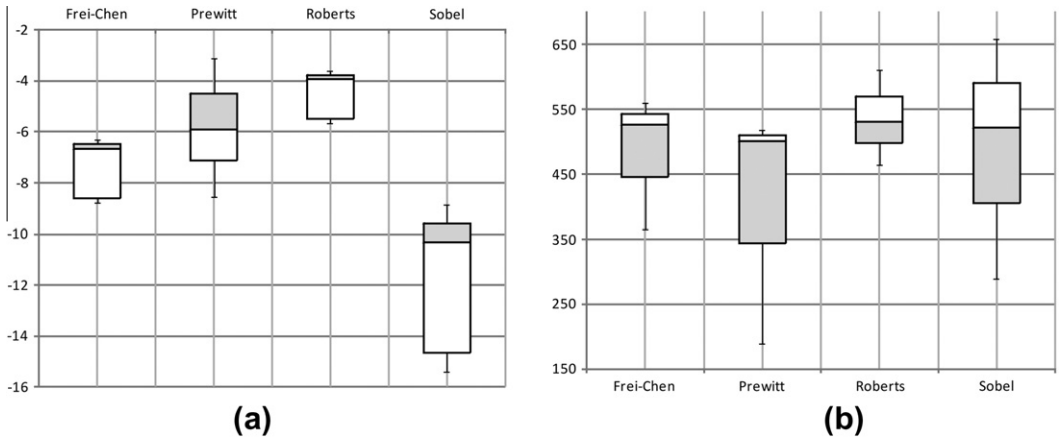

Fig. 14. Box-plot graphics of the coordinates of the vanishing point corresponding to the spatial *Y* axis. The *x* coordinate is shown in (a) and the *y* coordinate in (b). Values in millimeters.

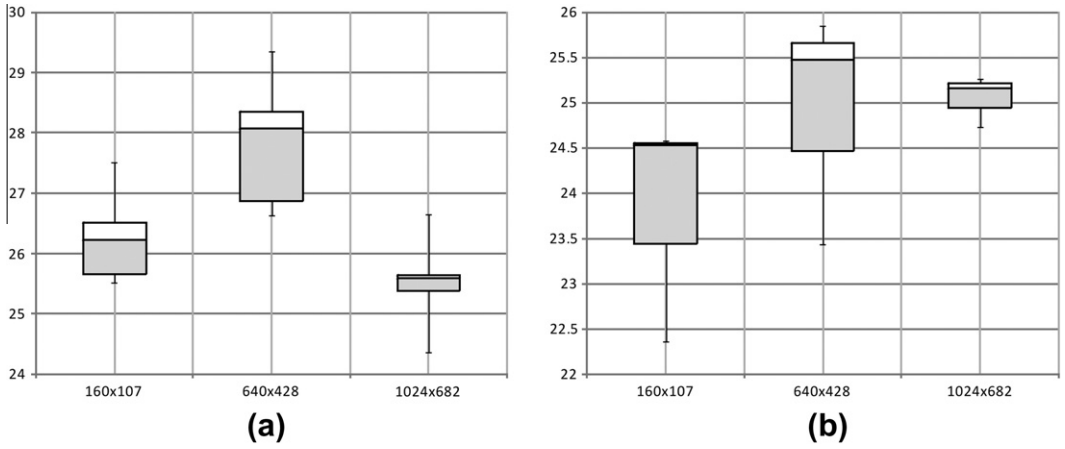

Fig. 15. Box-plot graphics of the coordinates of the vanishing point corresponding to the spatial *Y* axis. The *x* coordinate is shown in (a) and the *y* coordinate in (b). Values in millimeters.

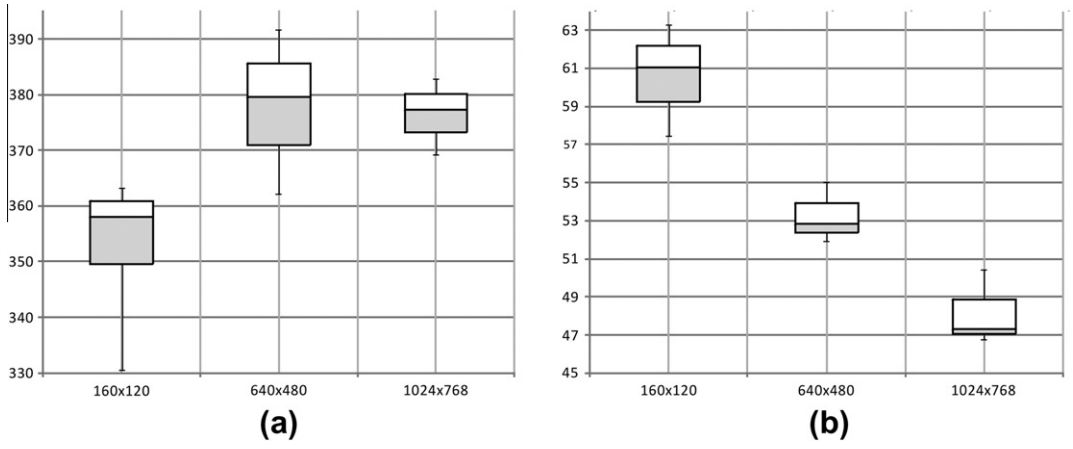

Fig. 16. Box-plot graphics of the coordinates of the vanishing point corresponding to the spatial *X* axis. The *x* coordinate is shown in (a) and the *y* coordinate in (b). Values in millimeters.

is centered on two differentiated aspects: the type of operator and the resolution used.

The statistical results have been obtained from the data provided by the algorithm developed and which refer to the circles adjusted to fit the point cloud. In order to compare the results, according to the type of operator or the resolution of the photograph, they are shown in box-plot graphics (Microsoft Excel).

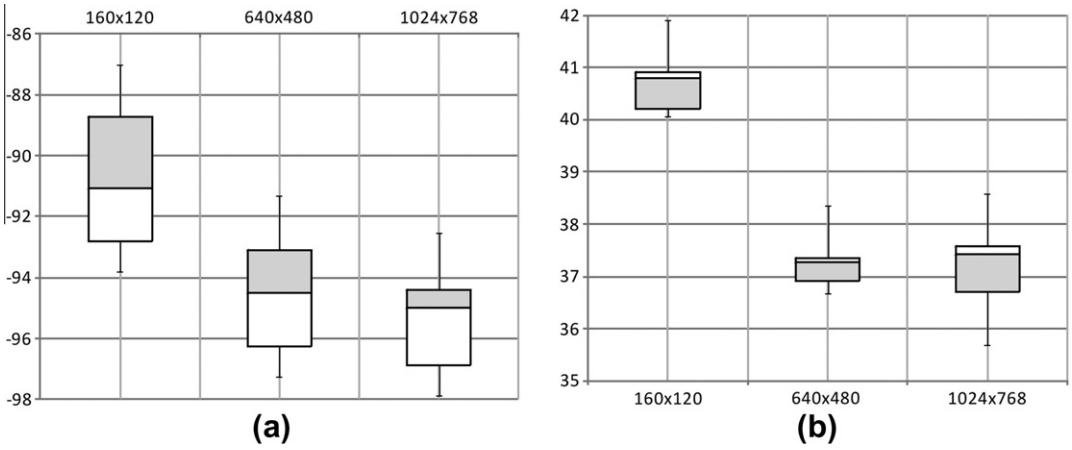

Fig. 17. Box-plot graphics of the coordinates of the vanishing point corresponding to the spatial *Y* axis. The *x* coordinate is shown in (a) and the *y* coordinate in (b). Values in millimeters.

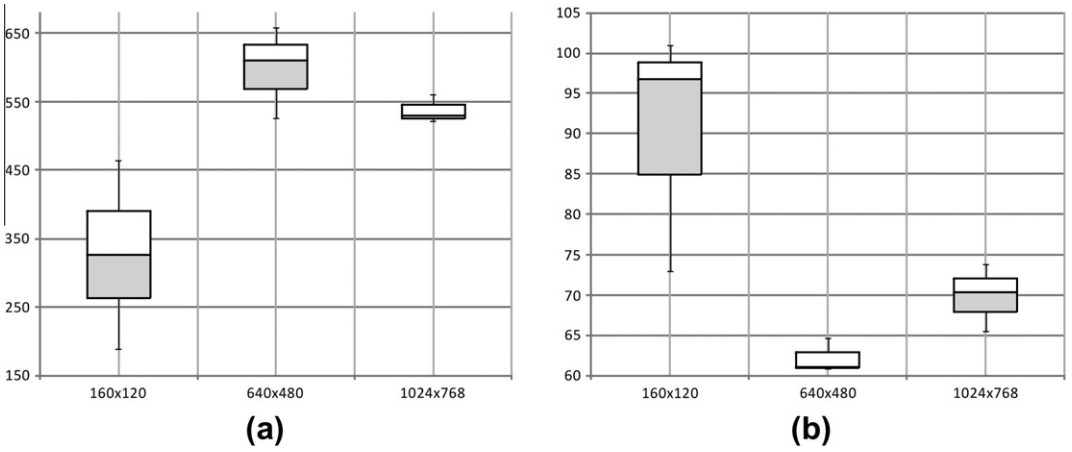

Fig. 18. Box-plot graphics of the coordinates of the vanishing point corresponding to the spatial *X* axis. The *x* coordinate is shown in (a) and the *y* coordinate in (b). Values in millimeters.

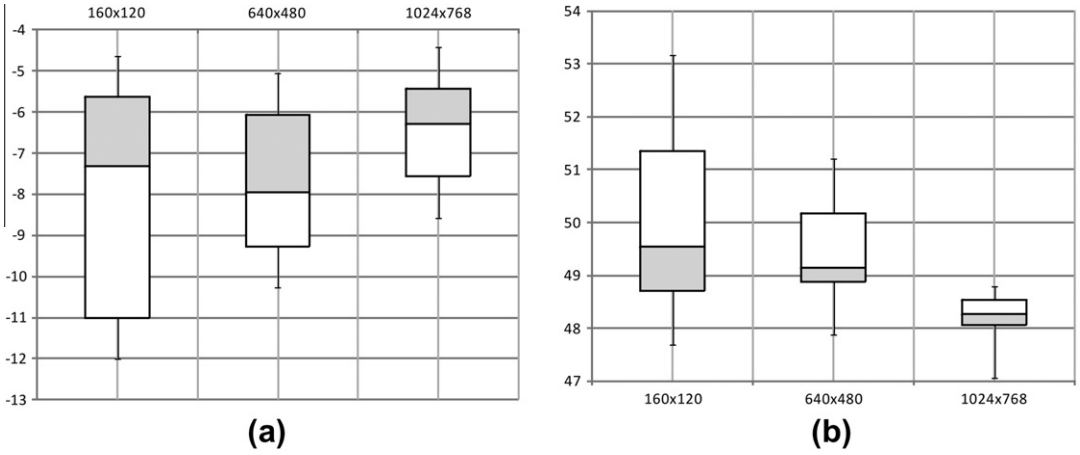

Fig. 19. Box-plot graphics of the coordinates of the vanishing point corresponding to the spatial *Y* axis. The *x* coordinate is shown in (a) and the *y* coordinate in (b). Values in millimeters.

4.1. Obtaining the vanishing point according to the edge operator

4.1.1. Perspective of a vanishing point

Fig. 10(b) shows a great dispersion of the results for the *y* coordinate, whereas for the *x* coordinate the results are more uniform (Fig. 10(a)). Comparing both figures, it can be concluded that Sobel's operator has the best performance, as it has the least dispersion of the values obtained.

4.1.2. Perspective of two vanishing points: case 1

4.1.2.1. Vanishing point corresponding to the spatial X axis. Fig. 11 shows that Prewitt's and Roberts' operators do not produce statis-

tically uniform results. However, Frei-Chen's and Sobel's operators offer similar values for the *x* coordinate, and the *y* coordinate shows that Frei-Chen's operator has the best performance.

4.1.2.2. Vanishing point corresponding to the spatial Y axis. In Fig. 12 the values obtained by Prewitt's and Roberts' operators show a large dispersion. However, Frei-Chen's and Sobel's operators have similar performance for the x coordinate, although the values of the *y* coordinate (Fig. 11(b)) show that Sobel's operator has the best performance.

4.1.3. Perspective of two vanishing points: case 2

4.1.3.1. Vanishing point corresponding to the spatial X axis. Fig. 13 shows a higher dispersion in the data obtained with Prewitt's and Sobel's operators. However, comparing the results obtained by applying Frei-Chen's and Roberts' operators, it is Roberts' operator which shows the lowest dispersion and therefore the best performance.

4.1.3.2. Vanishing point corresponding to the spatial Y axis. Fig. 14 shows a great dispersion of results when Sobel's operator is applied. The distribution of data is similar for Frei-Chen's and Roberts' operators, and it is notable that both show a strong bias in both coordinates: towards a minimum for the *x* coordinate and towards a maximum for the *y* coordinate. In this case, the best result is obtained with Roberts' operator, taking into account the size of the box and the symmetry in the distribution of the *y* coordinate.

4.2. Obtaining the vanishing point according to the resolution of the image

4.2.1. Perspective of a vanishing point

Fig. 15 shows that the boxes are asymmetric, and therefore, indicate that the data have a strong bias to the lower part, the minimum. It is interesting to note the similarity between the boxes in both figures, which shows that the performance of the values is almost identical irrespective of the coordinates. The configuration of the box-plot graphics for resolutions 106×107 and 640×428 is very similar, so the influence of the resolution is almost imperceptible. However, when the resolution is increased to 1024×682 pixels, the results are improved as the number of points in the cloud increases.

4.2.2. Perspective of two vanishing points: case 1

4.2.2.1. Vanishing point corresponding to the spatial X axis. Fig. 16 shows that the dispersion of data is greater for the *x* coordinate than for the *y* coordinate. The *x* coordinate value of the vanishing point is similar for resolutions 640×480 and 1024×768 (Fig. 12(a)), while the data show bias towards the minimum. Fig. 12(b) shows an opposite bias for the same resolutions. Therefore, it can be concluded that the increase in resolution improves the results.

4.2.2.2. Vanishing point corresponding to the spatial Y axis. Fig. 17 shows that the dispersion of data is greater for the *x* coordinate than for the *y* coordinate, and therefore the dispersion decreases as the resolution of the image increases. In this case, there is no excessive difference between the results obtained for resolutions of 640×480 and 1024×768.

4.2.3. Perspective of two vanishing points: case 1

4.2.3.1. Vanishing point corresponding to the spatial X axis. Fig. 18 shows how the dispersion of data decreases as the resolution increases, giving a briefer bias for the *x* coordinate than for the *y* coordinate of the vanishing point.

4.2.3.2. Vanishing point corresponding to the spatial Y axis. Fig. 19 shows that the dispersion of data is greater for the *x* coordinate than for the *y* coordinate, and that is decreases as the resolution increases.

5. Conclusions

This article has shown different detection methods for vanishing points. The results have been presented by applying an algorithm based on Thales' second theorem to photographs with different resolutions and numbers of vanishing points.

The study is centered on the comparison of four discrete gradient operators for edge detection (Frei-Chen, Prewitt, Roberts and Sobel), as well as on the observation of the influence of resolution on the results obtained.

The method applied in this paper has the advantage of being accurate, reliable and simple, although the computational requirements associated with edge detection and line extraction increase with higher resolutions. However, determining the coordinates of vanishing points has a low computational cost.

From the study of the results the following can be deduced:

- Frei-Chen's operator gives good results for determining vanishing points with respect to the spatial *X* axis.
- Sobel's operator is the most appropriate for determining vanishing points with respect to the spatial *Y* axis.
- Roberts' operator shows good results for calculating vanishing points in both spatial axes.
- Prewitt's filter is not appropriate for processing this type of images.
- Increasing the resolution of the image improves results. This is most evident for images with a resolution of 1024×768 pixels.

Accurate knowledge of the position of vanishing points allows for virtual reconstructions from monoscopic measurements. Therefore, the results obtained in this research will allow the algorithm to be improved, with the objective of using Thales' second theorem in low resolution images, and in images where the internal orientation parameters are unknown, as in images which are found on the internet.

References

Almansa, A., Desolneux, A., & Vamech, S. (2003). Vanishing point detection without any a priori information. *IEEE Transactions on Pattern Analysis and Machine Intelligence, 25*, 502–507.

Barnard, S. (1983). Interpreting perspective images. *Artificial Intelligence, 21*, 435–462.

Bovik, A. C. (2009). *The essential guide to image processing*. London: Academic Press.

Burns, J. B., Hanson, A. R., & Riseman, E. M. (1986). Extracting straight lines. *IEEE Transactions on Pattern Analysis and Machine Intelligence, 8*, 425–455.

Collins, R. T., & Weiss, R. S. (1990). Vanishing point calculation as a statistical inference on the unit sphere. In *Proceedings of the 3th international conference on computer vision* (pp. 400–403).

Gamba, P., Mecocci, A., & Salvatore, U. (1996). Vanishing point detection by a voting scheme. In *Proceedings of the conference on image processing* (pp. 301–304).

Gander, W., Golub, G. H., & Strebel, R. (1994). Least-squares fitting of circles and ellipses. *BIT Numerical Mathematics, 34*, 558–578.

Kalantari, M., Jung, F., Paparoditis, N., & Guedon, J.P. (2008). Robust and automatic vanishing points detection with their uncertainties from a single uncalibrated image, by planes extraction on the unit sphere. In *The international archives of the photogrammetry, remote sensing an spatial information sciences, XXXVII Part B3a* (pp. 203–207).

Kalantari, M., Jung, F., & Guedon, J. P. (2009). Precise, automatic and fast method for vanishing point detection. *The Photogrammetric Record, 24*, 246–263.

Kang, D. J., & Jung, M. H. (2003). Road lane segmentation using dynamic programming for active safety vehicles. *Pattern Recognition Letters, 24*, 3177–3185.

Magee, M. J., & Aggarwal, J. K. (1984). Determining vanishing points from perspective images. *Computer Vision, Graphics and Image Processing, 26*, 256–267.

McLean, G. F., & Kotturi, D. (1995). Vanishing point detection by line clustering. *IEEE Transactions on Pattern Analysis and Machine Intelligence, 17*, 1090–1095.

Palmer, P. L., & Tai, A. T. (1993). An optimized vanishing point detector. In *Proceedings of the British machine vision conference* (pp. 529–538).
Schaffalitzky, F., & Zisserman, A. (2000). Planar grouping for automatic detection of vanishing lines and points. *Image and Vision Computing, 18*, 647–658.
Straforini, M., Coelho, C., & Campani, M. (1993). Extraction of vanishing points from images of indoor and outdoor scenes. *Image and Vision Computing, 11*, 91–99.
Tai, A., Kittler, J., Petrou, M., & Windeatt, T. (1993). Vanishing point detection. *Image and Vision Computing, 11*, 240–245.
Wang, J., Lin, C., & Chen, S. (2010). Applying fuzzy method to vision-based lane detection and departure warning system. *Expert Systems with Applications, 37*, 113–126.